
Article:
Rodgers, A, de Boer, G orcid.org/0000-0002-5647-1771, Murray, B orcid.org/0000-0002-6493-1547 et al. (2 more authors) (2019) An investigation in to batch cleaning using wash racks. Food and Bioproducts Processing, 113. pp. 118-128. ISSN 0960-3085

https://doi.org/10.1016/j.fbp.2018.11.003

An investigation in to batch cleaning using wash racks

Alistair Rodgers[1*], Greg de Boer[1], Brent Murray[2], Gordon Scott[3], Nikil Kapur[1]

[1]School of Mechanical Engineering, University of Leeds, Woodhouse Lane, Leeds, LS2 9JT, UK.
[2]School of Food Science and Nutrition, University of Leeds, Woodhouse Lane, Leeds, LS2 9JT, UK.
[3]GlaxoSmithKline, Harmire Road, Barnard Castle, DL12 8DT, UK.
*Corresponding author. Email: mn11a2r@leeds.ac.uk; Tel: +44(0) 7463 234 462.

Highlights

- Flow distribution through washing racks modelled using a pipe network approach.
- Exploration of the mechanism of removal of white soft paraffin on a vertical wall.
- Growth of clean area restricted by ridge of accumulated material displaced by the jet on perimeter of the clean area.
- Material transported to the ridge via a rolling mechanism.
- Cleaning efficiency analysis from an energy perspective.

Abstract

Batch cleaning processes, using washing racks, were studied in two distinct phases; the distribution of flow within the rack to the formation of jets at the nozzles and the interaction of the jetted fluid with the surface. A pipe network approach was used to model the flow in the rack and the interaction of the fluid with the surface was studied using a specifically designed test rig. A stationary coherent jet was set up to impinge horizontally on to a vertical wall. White soft paraffin (WSP) was used as the soil material, an excipient commonly used in pharmaceutical processing. Three variables (flow rate, WSP thickness and water temperature) were controlled and chosen to match the conditions on an exemplar wash rack. Water with no added surfactant was used for all experiments. Flow rates were in the range 1 – 4 l min^{-1} which corresponded to Re = 5960 – 23840 for the 4 mm diameter jet used. The limits of WSP thickness and water temperature were set between 0.19 to 1.9 mm and 20 to 60 ˚C, respectively. Clean areas produced by each jet were measured using image processing and using this data the cleaning performance of each system was compared against each other. An energy framework was adopted to allow cleaning to be assessed in terms of efficiency which provides a framework for optimisation of the process.

Keywords

Batch cleaning, white soft paraffin, impinging jet, soil removal mechanisms, efficiency

1 Introduction

The cleaning of production equipment is a significant yet frequently overlooked aspect of the batch manufacturing cycle. Cleaning as a process has been described as a mixture of four factors which combine to form the quadrants of Sinner's circle; mechanical action; chemical action; cleaning time; and temperature (Sinner, 1959). Encapsulated within this is the shape and roughness of the surface, the rheology of the product to be cleaned, the choice of surfactant and the nature of the interaction of the spray or jet with the product, for example miscible or immiscible. Fryer et al. (2009) categorised cleaning problems in terms of cost and complexity of the soil by classifying them as (i) viscoelastic or viscoplastic fluids such as yoghurt that can be rinsed from a surface with water; (ii) microbial and gel-like films which require both water and a chemical agent; (iii) solid-like cohesive foulants that require mostly chemical removal. Cleaning was also classified by Fryer et al. (2009) in terms of the cleaning mechanisms which can be employed for a given system. They suggested that cleaning must first overcome cohesive forces that bind the material together and secondly adhesive forces between the

deposit and the surface. This can be done by fluid action alone (fluid mechanical removal) or through a combination of fluid and chemical mechanisms (diffusion-reaction removal). With the latter, cleaning involves diffusion of the chemical to and/or into the deposit and a physicochemical reaction that transforms the deposit to a removable form.

To better understand the hydrodynamics of cleaning, Wilson et al. (2012, 2014) considered the impingement of a jet on a vertical wall. Experimentally they observed three key regions (see Fig. 1.1) - (i) the radial flow zone (RFZ) where a thin, fast moving layer of fluid exerts a shear stress on the surface, (ii) a rope like jump which bounds the RFZ, termed the film jump and (iii) a falling film that drains from the film jump. Drosos et al. (2004) described how the flow in the falling film develops from an initially uniform liquid layer with a smooth surface, to a complex state in which two-dimensional waves first appear, eventually developing further downstream into larger three-dimensional waves.

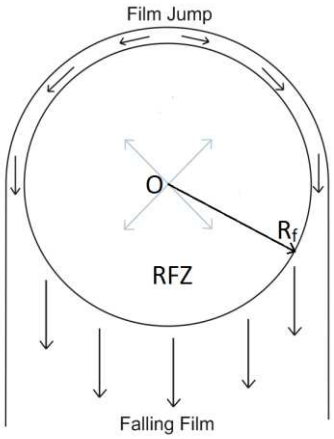

Fig. 1.1: Horizontal jet impinging on a vertical wall displaying the impingement point, O, radial flow zone, RFZ, the film jump and falling film. R_f is the radius of the film jump

In addition to considering the hydrodynamics, the behaviour of the soil removal was also considered, with three identified mechanisms that can often occur in parallel with each other:

i. Dissolution, where the jetted fluid solvates the product.
ii. Erosion, where the jet causes the product to be broken down due to hydrodynamic forces.
iii. Soaking, whereby when the soil is insoluble and prolonged contact with the solvent promotes a change in the microstructure of the layer such that one of the previous mechanisms can occur. This is the predominant mechanism in the falling film due to the shear stress exerted on the wall being lower in this region.

In most industrial applications the liquid is not pure water and will contain a surfactant. Surfactants remove oily soils from a substrate through a roll-up mechanism, in which the contact angle between the soil and the substrate is increased by adsorption of the surfactant. These surfactants can be independent or in aggregate forms called micelles. This causes a reduction in work required to move the soil from the substrate (Rosen et al., 2012). Tailby et al. (1961) observed that the presence of surfactants have an effect on the hydrodynamics of the falling film. A concentration of as little as 0.005% was enough to substantially dampen the amplitude of the waves experienced downstream of the source of the flow. Typical surfactant concentrations in the pharmaceutical industry range between 1-2% however this can be doubled for soils that are particularly difficult to remove (McLaughlin et al., 2005).

With batch cleaning, control is required to manage residues between batches of product, particularly when multiple products are made using the same equipment (Lakshmana Prabu et al., 2010). With batch processing, equipment is commonly disassembled in to its constituent parts which are then loaded on to a washing rack for cleaning-out-of-place (COP) (PMTC, 2015). Each washing rack comprises a series of pipes and nozzles through which a mixture of (often heated) water and surfactant

passes. The nozzles are positioned such that the fluid flow cleans the loaded components via a jet or spray.

Batch processing is prevalent within pharmaceutical manufacture where the active pharmaceutical ingredient is manipulated into a dose form suitable for human use e.g. creams and ointments. Within this sector, after the cleaning process has taken place, the parts are inspected and must meet cleanliness acceptance criteria with limits for cleaning validation established by the manufacturer and a regulatory body. A visually clean criterion, whereby after inspection the part appears clean to the naked eye, is a minimum requirement for acceptance and is limited by the Food and Drug Administration (FDA) to use between lots of the same product, in other cases it must be used in conjunction with other criteria (FDA, 1993). Said criteria include (Lakshmana Prabu et al., 2010);

i. Swab tests; in which the contaminant must not typically exceed a concentration of 10 parts per million in the subsequent batch.
ii. Dose criterion, where no more than 0.1% of minimum daily dose of any product will appear in the maximum daily dose of another.
iii. Maximum Allowable Carry-Over (MACO), where the limits for carryover of product residues are based on a toxicological evaluation.
iv. Health based limits; determine that no more than the acceptable daily exposure of the product being cleaned appears in the maximum daily dose of the next product being manufactured. The limit is the amount of active substance that a person can be exposed to as a contaminant in another product without experiencing any adverse health effects (PMTC, 2015).

While regulations and guidelines vary from country to country, they are designed to ensure the safety, efficiency and security of the pharmaceutical product being manufactured. Good practice is used to identify common failures and the cleaning process amended to address these (PMTC, 2015). This can be a source of inefficiency to a manufacturer since additional maintenance costs and costs due to production loss are incurred. In the event of products cross-contaminated from previous batches having to be recalled, incurred costs include product rehabilitation costs, recall costs and costs of interruption to business. Shewale et al. (2014) valued this to be 49% of the total recall cost. Between 2001 and 2014 the FDA reported more than 1,984 recalls in the pharmaceutical industry with more than $700 million manufacturer's penalties and billions more lost in revenue (Shewale et al., 2014).

This study addresses batch cleaning of components where COP is frequently used. Here parts are removed from the process equipment and loaded onto racks which incorporate a series of nozzles, before undergoing a series of distinct cleaning operations. Whilst both jets and sprays are used in COP processes, this work focuses on the former. Although the focus is on COP; many of the findings from this study will be applicable to cleaning-in-place (CIP), where production equipment is cleaned in-situ. This work studies hydrodynamic cleaning from a wash rack into two distinct phases: (i) the distribution of the flow within the rack to the formation of jets at the nozzle, (ii) the interaction of the fluid with the surface. The aim of this research is to seek more optimal flow conditions on washing racks used in COP in the pharmaceutical industry to ultimately improve their efficiency and efficacy in meeting cleaning validation criteria set out by the industry. The work is novel in its approach as it is applied to wash racks used in the pharmaceutical industry, which have not been studied in great detail, the soil used for experiments is an excipient commonly used in the manufacture of pharmaceuticals and an energy framework has been adopted to evaluate the efficiency of different jets. The output from the research can be utilised and applied directly to industry.

2 Materials and Methods

2.1 Distribution of flow within the rack

2.1.1 Wash rack characterisation

A typical wash rack employed in cleaning components, for example those used during the manufacture of pharmaceutical products, is shown in Fig. 2.1. This rack is loaded with disassembled parts off the manufacturing line, before being coupled to a pump which distributes flow through the hollow structure to the nozzles. The nozzles are positioned to impinge on components to remove any soil. Custom racks are used to ensure the cleaning of a component is uniform from batch to batch and thereby allowing a validated process to be established. The principle of poka-yoke (Shimbun, 1988) is often employed to minimise operator error around loading racks to ensure specific parts sits in the same location (in relation to the jet) each time it is cleaned. There are no formal methods available to study the fluid flow distribution within a rack and no methodical way of choosing the correct jet characteristics for each nozzle, this is generally undertaken based on observed behaviour of the cleaning process on plant. There is a requirement for an analytical approach to support nozzle selection.

Fig. 2.1a: Wash rack unloaded. Each pipe section can be seen leading to a nozzle on to which a component is loaded

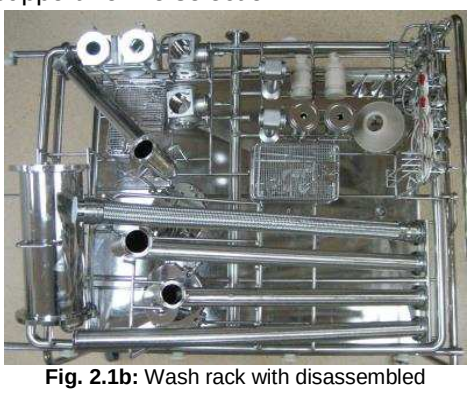

Fig. 2.1b: Wash rack with disassembled components loaded on to jet/spray nozzles

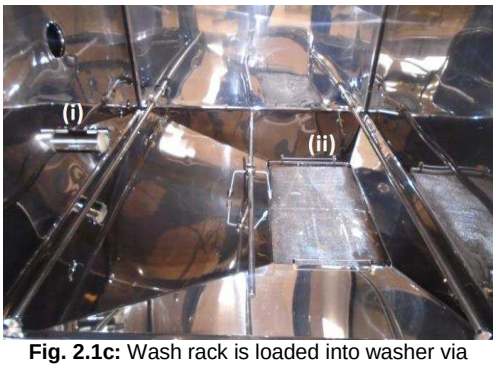

Fig. 2.1c: Wash rack is loaded into washer via coupling (i), water is recirculated via sump (ii)

Described next is a method for describing the flow network from the pump, through the rack and to the nozzles in order to better understand: (i) the overall flow distribution; and (ii) the ranges of flow rate from jets on a suitable washing rack. This is undertaken as a way to evoke hydrodynamic studies of the individual jet-surface interaction in the correct parameter space and as a design methodology for analysing wash racks.

Fluid flow through the wash racks was modelled by application of the conservation of mass and momentum under steady-state, incompressible and isoviscous conditions. The water-surfactant mixture present in the wash racks was assumed to have the same properties of water at standard operating conditions. For the distribution studies, a pipe network approach was used to predict flow distribution, utilising the open source software EPANET (United States Environmental Protection Agency, 2016).

EPANET was developed by the Environmental Protection Agency (EPA) in the United States for the purpose of modelling hydraulic and water quality behaviour in water distribution systems. EPANET is based on the Bernoulli approximation and flow continuity which facilitates equations to be derived relating each node in the flow network, the resulting matrix problem is solved using a variant of the Newton-Raphson method known as the gradient method (Todini and Pilati 1988). The approach employed assumes frictionless pipe sections to simplify the model specification with tests carried out to show this was a reasonable assumption for this rack. Based on a typical wash rack chosen to exemplify the method, the geometry of the pipe network (diameter, length and connectivity) was created (see Fig. 2.2), this describes the interconnections between the pump inlet and the nozzle outlets. For reference the size of the pipe sections were specified as follows: the main feed was 40 mm in diameter; and all sections protruding from the main feed were 22 mm in diameter. In Fig. 2.2 the main feed is shown by the vertical line section in bold.

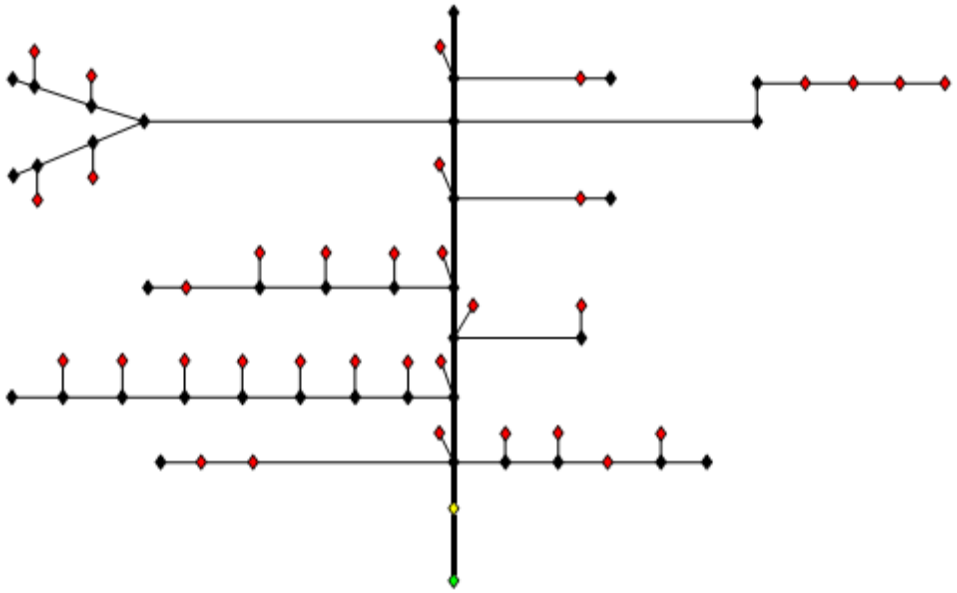

Fig. 2.2: Idealised flow network of an example wash rack. Main feed shown by the vertical, bold line. Pipes and connecting sections (black), nozzles (red), pump (green), coupling (yellow)

2.1.2 Nozzle Characterisation

Each nozzle on the wash rack was characterised by defining a discharge coefficient k (l $min^{-1}Pa^{-0.5}$) based on a measured flow rate Q (l min^{-1}) versus pressure drop ΔP (Pa) relationship. The model defining the discharge coefficient is described by equation 2.1, in order to determine k for a specific nozzle, a hydraulics bench circuit was set up to allow control of the volumetric flow through the nozzle. A digital manometer was used to give the pressure difference over the nozzle for a range of flow rates. Subsequently the square root of the pressure drop was plotted against the flow rates with the gradient of the linear regression corresponding to k (Rossman, 2000).

$$Q = k\Delta P^{0.5} \tag{2.1}$$

Manufacturers do sometimes provide this data for nozzles in data sheets however it is not always possible to find this information for all nozzle types, additionally it is often the case that nozzles are made in-house and the discharge coefficients are not known. A comparison between manufacturer data and experiments performed in a laboratory gave a typical difference of ~5-7%.

2.1.3 Pump/coupling characterisation

It was known for the wash rack modelled here (Fig. 2.1), that the pressure downstream of the coupling (the yellow node in Fig.2.2) is 140 kPa, which was determined in-situ on site during quality assurance processes. Equating the pressure downstream to this in the EPANET model allows the subsequent flow through the rack to be calculated using the method outlined in 2.1.1.

In order to extend the model to include the coupling, which itself has a degree of leakage so as to self-clean and prevent soil build up on the interlocking section, the characteristics of the pump would need to be included (the pressure / flow rate relationship) – either from a manufacturer's data sheet or through experimentation. This would then provide data of leakage from the coupling.

2.2 Jet apparatus

2.2.1 Test rig design

To investigate the cleaning characteristics of the jets on the rack, a coherent jet was visualised on a test apparatus. This was designed and built where a stationary coherent jet was positioned to impact perpendicular to a transparent wall made from Perspex. The nozzle used was 4 mm in diameter with a discharge coefficient of 0.032 l min^{-1} $Pa^{-0.5}$. The standoff distance of the nozzle from the wall was set to a specified value, d. Behind the transparent wall, a Logitech C920 camera was positioned so that the cleaning process could be observed and recorded. The water, the flowrate of which was measured using a rotameter, was recycled through a collection tank. To ensure the water was not contaminated it was replaced at regular intervals. The tank was covered with a nitrile rubber thermal insulating sheet of 25 mm thickness and a thermal conductivity of 0.034 W $m^{-1}K^{-1}$ to ensure that the water remained a stable temperature during heated experiments. Fig. 2.4 shows a schematic diagram of the test rig and Fig. 2.5 a photograph of the experimental apparatus.

It is important to note that the test apparatus assumes a flat surface perpendicular to the jet, however frequently on the wash racks there is actually curvature of the surfaces loaded on to them. In addition to this jets do not always impinge perpendicular to the surfaces being cleaned; there can often be an angle of incidence. In this work these factors have not been studied in order to simplify the problem. The use of Perspex as the surface material is also a simplification of the cleaning process observed on the wash racks since most production equipment used in the pharmaceutical industry is stainless steel. Perspex was chosen for its transparency thus allowing for relative ease of filming the cleaning process. Water with no added surfactant was also used as a simplification of the cleaning process as surfactant is often used on wash racks. This will form the focus of future studies.

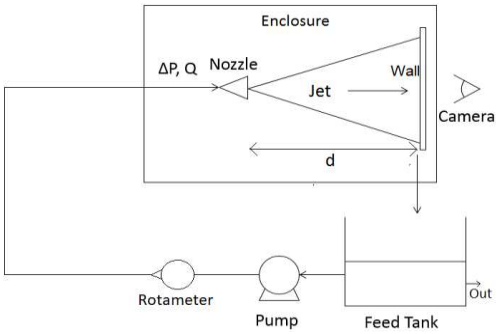

Fig. 2.4: Test rig schematic; the arrows represent the flow of water. The enclosure and wall are both made of Perspex to allow for easy observation and imaging from the camera. ΔP and Q represent pressure drop across the nozzle and flow rate respectively

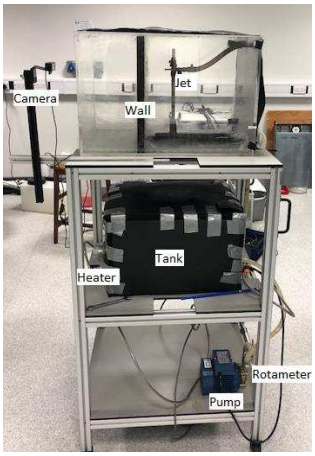

Fig. 2.5: Photograph of test apparatus with main components identified

2.2.2 Design of experiments

The experiments were designed such that the variables to be studied were flow rate, standoff distance of the nozzle, soil thickness and water temperature.

In order to operate on the test rig under conditions that match those experienced on the wash racks as closely as possible, typical distances from the surface to the jet were to be determined. This was achieved by examining a range of cleaning racks on a pharmaceutical manufacturing site. By looking closely at the racks it was possible to identify the typical size of the components that are loaded on to them and measure the distance between the surface being cleaned and the nozzle. The parts loaded on to the racks varied from small diameter pipes to larger components such as filling machine pressurised header tanks. Typically standoff distances varied between approximately 50 mm to 200 mm. Early experiments in this design space showed that the standoff distance had very little effect on cleaning performance and was therefore disregarded as a variable. All further experiments were conducted at a 50 mm standoff.

To efficiently fill the design space a Box Behnken design for the remaining three variables was used (Box et al., 1960). Three points were used to fill the design space for each variable.

Flow rates were matched to those on the wash rack using the data generated by EPANET using the method outlined in 2.1.1. As will later be presented in section 3.1, flow rates on the rack varied between 2 and 40 l min^{-1}. The mean, median and mode flow rates respectively on the wash rack are 10.4 l min^{-1}, 5.4 l min^{-1} and 4.2 l min^{-1}, respectively. The pump used on the rig was selected to study flow rates in proximity to the modal nozzle flow rate. This research focused mainly on the cleaning of smaller components and not larger components which demanded the higher flow rates seen on the rack, the lower boundary of the flow rates was thus explored. Operating flow rates on the test rig were 1, 2.5 and 4 l min^{-1}.

Water temperatures were selected as 20 ˚C, 40 ˚C and 60 ˚C, the latter two of which encompass the melting point of the soil under study.

2.3 Material characterisation

2.3.1 White soft paraffin

The soil material chosen for experiments was white soft paraffin (WSP), an excipient commonly used in pharmaceutical processing. WSP is commonly used in the manufacture of ointments which are applied to the body for dermatological use. No other materials were used in this study. The WSP was applied to the Perspex wall by drawing down an excess of WSP with a straight edge, using tape of thickness 0.19mm either side of the wall to meter the thickness. The thickness of the WSP could then be controlled through using multiple layers of tape. It is reasonable to assume that the error in applied thickness is small enough to be considered negligible. The typical area of WSP applied to the Perspex wall for each experiment was approximately 35000 mm^2. Residual soil thicknesses in batch cleaning can vary, depending on operation and whether excess material is manually removed before loading onto the wash rack. Based on observation, a range of WSP thicknesses were selected for study, these were 0.19 mm (t), 0.95 mm (5t) and 1.9 mm (10t), where t represents the thickness of the tape.

2.3.2 White soft paraffin characterisation

To characterise the WSP used for cleaning, penetration tests were conducted. The penetration test indicates the force required to penetrate the sample. It is commonly used in the pharmaceutical industry to test WSP and is part of standardised quality testing for WSP (Pharmacopoeia, 2005). The tests were conducted on a TA-XT Plus texture analyser (Stable Micro Systems, UK). A flat metallic probe of 10 mm diameter was positioned above the sample and lowered at a constant speed of 0.5 mms^{-1} to a

depth of 2 mm below the surface of the WSP. Once the penetration distance had been reached, the probe was withdrawn at a constant speed of 5 mm s^{-1}. This test was then repeated in 4 different locations on the sample and an average force – distance curve plotted. The test was conducted at room temperature 20 ˚C.

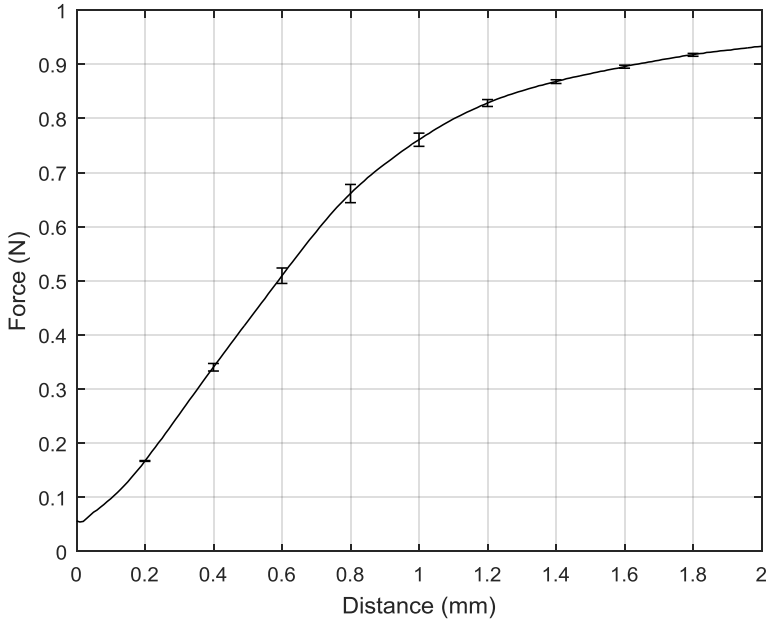

Fig. 2.6: Penetration test Force versus Distance plot (measured at 20˚C) Error bars plotted using standard deviation

Fig. 2.6 shows how the gradient of the Force vs Distance curve decreases with increasing distance under the surface of the WSP. Using this curve, the force required to penetrate the WSP to the surface of the wall can be extrapolated for each WSP thickness. An initial force of approximately 0.06 N is required for the WSP to yield and penetration to occur. For the 0.19 mm, 0.95 mm and 1.9 mm WSP thicknesses respectively, and assuming no interaction of the solid support surface the forces required to penetrate the entire soil layer are approximately 0.16 N, 0.74 N and 0.93 N. The drop point temperature range of the WSP was given on a manufacturer's data sheet as between 35 – 70 ˚C, but DSC analysis by Bentley (2017) shows a large melting peak at 30-40 ˚C.

2.4 Image processing

The recordings from the camera positioned behind the Perspex were used to calculate the area of WSP removed as a function of time. This was done using ImageJ, an open source image processing software (Rasband, 1997). Still images were taken from the videos at specified time points. The images were scaled in ImageJ to a known distance which was the distance between the pieces of tape described in 2.3.1. Each pixel was thus assigned a scale and each clean area could be measured using an analysis tool in ImageJ. The tool allows the user to draw freehand around the shape of the clean area and subsequently measure the size of the enclosed area. This was then plotted against its corresponding time.

2.5 Energy input calculations

The power input, W (W), across the nozzle is given by the product of pressure drop and flow rate, given by equation 2.2 (Engineering ToolBox, 2004).

$$W = Q\Delta P \tag{2.2}$$

Substituting 2.1 into this gives the power input in terms of two known quantities, Q and k, given by equation 2.3.

$$W = \frac{Q^3}{k^2} \tag{2.3}$$

where ΔP is the pressure drop across the nozzle (Pa) and Q is the flow rate (m^3s^{-1}). The energy input was then calculated by taking the product of power and time. Calculating the energy input with respect to time allowed for the WSP removal to be plotted against energy input and this subsequently gauged the efficiency of each experiment.

3 Results and Discussion

3.1 Flow network analysis

The distribution of flow through the wash rack is presented in Fig. 3.1. Table S1 can be found in the supplementary data which presents the flow rate data and percentage distribution through each nozzle. Fig. 3.1 depicts the flow network diagram (Fig. 2.2) as a bubble plot with additional circles included (in blue) for which the area is proportional to the magnitude of flow rate passing through the nozzles.

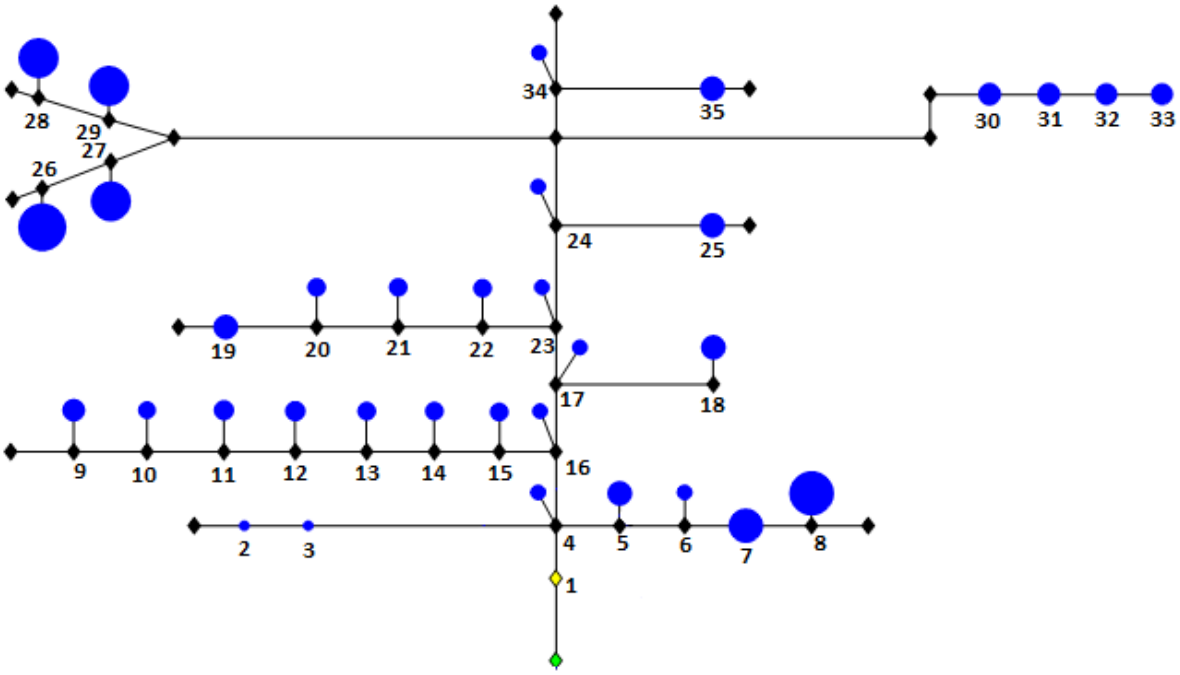

Fig. 3.1: Bubble plot showing the distribution of flow rates in wash rack with each nozzle ID labelled. Flow rates proportional to nodal areas (blue), coupling left unfilled. Flow rate data and percentage distribution through nozzles can be found in Table S1 in supplementary data

This is a powerful visualisation of the wash rack flow rates because it allows the user to observe the nozzles which are either over or under supplied with fluid. For instance if parts loaded on to particular nozzles are regularly failing cleaning validation, the relevant nozzles can be identified in Fig. 3.1 to see if this is due to the nozzle being under-supplied. This then allows for an iterative approach to be made in-silico by optimising the nozzle selection for improved flow distribution.

An assessment was made to include the pump curve, allowing the cleaning flow of the coupling to be estimated. However, the pump data of the commercial rack and losses internal to the washer piping before the coupling were not available. From the pump nameplate, the total flow was given as 2000 l

min^{-1}, and this with a range of zero-flow pressures, was used to evaluate possible losses through the coupling. For the analysis for the pump curve, considered (Fig. S1 supplementary) showed that the discharged flow through the coupling was as high as 1610 l min^{-1} and the total flow through the wash rack given as 2000 l min^{-1} (82.0 % of the total flow), as shown in column two of Table S1. The pressure upstream of the coupling was such that for the pressure downstream of the rack to match that which was measured in-situ (140kPa) the discharge coefficient required for the coupling was 0.044 l $min^{-1}Pa^{-0.5}$. Visual observations showed this is significantly greater than that seen in practice. By lowering the zero-flow pressure in the pump closer to the value measured downstream of the coupling, it was possible to lower the discharge coefficient of the coupling to a more realistic value. For example, a zero-flow pressure in the pump of 147 kPa (50% of the initial value) gives a reduction in total flow through the rack to 824 l min^{-1} and now 57% of the flow (470 l min^{-1}) discharged through the coupling. Although this still appears rather excessive, it does show the potential to include coupling loss if the full pump curve is available.

It is important to note that the rest of the flow through the rack is independent of the pump/coupling, so long as the pressure downstream of the coupling is known and applied to the EPANET model. Thus the bubble plot of Fig. 3.1 is fully representative of the rack under study. The total flow downstream of the coupling is 354 l min^{-1} and the percentage distribution through each nozzle can be found in Table S1.

3.2 Visualisation of soil removal

A time lapse of the cleaning process recorded from the camera placed behind the Perspex wall is shown in Fig. 3.2, for the 4 l min^{-1} jet on a 0.19 mm WSP thickness, at 20 ˚C.

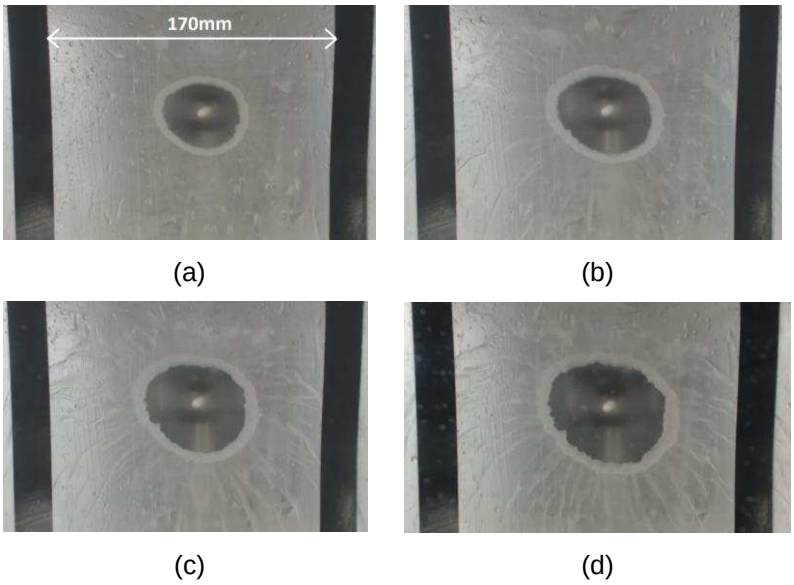

Fig. 3.2: Time lapse removal for 4 l min^{-1} jet and 0.19 mm WSP thickness (a) 3 s (b) 10s (c) 30 s (d) 300 s. Temperature 20 ˚C

Fig. 3.2 shows how as the jet impinges in the centre of the surface, the WSP is pushed radially outward forming a clean zone that grows with time. It is clear from the time lapse that the rate of change of the clean area is much higher at the start of the process and decreases with time. It can also be observed that as the process develops the ridge of WSP on the perimeter of the clean zone increases in thickness in the direction parallel to the wall.

To elucidate the soil removal mechanism, a study was conducted whereby an experiment was run for approximately 1 minute, before being paused, and then the base of the ridge dyed with an oil soluble

dye. The experiment was then continued for two more minutes to see where the dye had been displaced to, thus showing its path and the mechanism of its removal. This is shown in Fig. 3.3a and 3.3b.

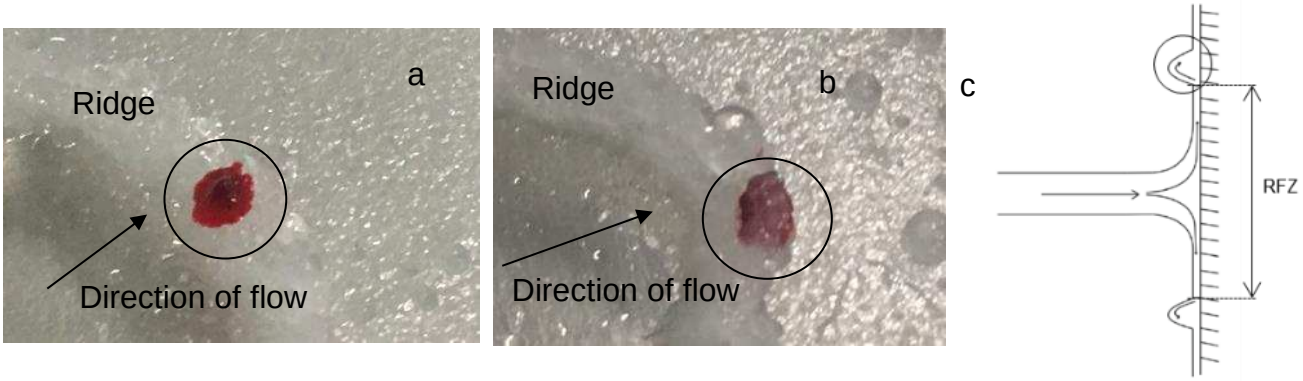

Fig. 3.3: (a) Dyed ridge of WSP at 60s (b) Dyed ridge of WSP after 180s (c) Adhesive soil removal and build-up of the ridge of WSP on the perimeter of the clean radial flow zone

It can be observed that the dye has been pushed to the back of the ridge and submerged under the ridge by the movement of the WSP. This suggests a rolling mechanism takes place, where the WSP at the edge closest to the radiating water film is pushed up and over to the back of the ridge. This process happens continuously, submerging the dye – shown schematically in Fig. 3.3c. The mechanism is continuous as the ridge builds in size and acts as a resistance to the radial flow produced by the jet which eventually restricts the final clean area, reducing the area theoretically derived on a clean surface by Wilson et al. (2014). Since the shear stresses exerted on the layer decrease with increasing distance from the impingement point, they are no longer large enough to overcome the adhesive force between the layer and the surface. At this point no adhesive removal can occur and the growth of the clean area reaches a standstill. A mass balance before and after the cleaning process revealed that only 17% of material had actually been removed from the surface, showing that most of the WSP is simply transported to the ridge. For material to be fully removed additional heat and/or surfactant need to be added to the system.

3.3 Clean Area vs Time and Energy Curves

Using the captured images, the area at a series of time intervals was calculated using ImageJ and subsequently plotted against time. Fig. 3.4 shows the growth of clean area as a function of time for each flow rate.

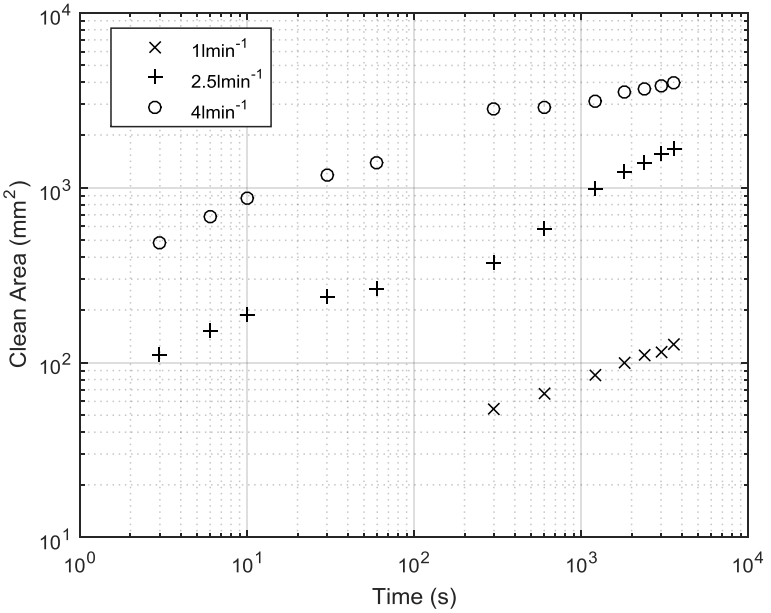

Fig. 3.4: Clean Area vs Time for each flow rate (0.19 mm WSP thickness, 20˚C)

Repeat preliminary experiments showed that errors between repeats typically did not exceed 10%. For each jet the soil is first removed cohesively as the jet has to break down the layer by the force exerted normal to the surface. For the two higher flow rates this occurs almost instantly, however the 1 l min^{-1} takes considerably longer due to the impingement force being lower, thus why no data points are shown for the 1 l min^{-1} jet in the first 100 s of cleaning. Once the jet in each case has reached the surface a liquid film is created that moves radially outwards and the removal mechanism becomes adhesive, where the soil is rolled over the surrounding material via the mechanism shown in Fig. 3.3c. The 4 l min^{-1} jet shows a very sharp increase in clean area during the first minute of cleaning. Close to the impingement point the shear stress exerted on the wall is at a maximum, consequently the adhesive removal occurs very rapidly. The 2.5 l min^{-1} jet shows a similar behaviour, but with a much more gradual rate of removal over the remainder of the process and not the sharp plateau that is observed in the 4 l min^{-1} case. The 1 l min^{-1} does not exhibit rapid removal in the early stages of cleaning as the shear stress exerted on the wall is relatively low.

The clean area after one hour of cleaning is now denoted by A*, this is a time significantly greater than the time of a single cleaning step experienced on the wash racks (one hour as opposed to a cleaning cycle of <10 min). These are estimated to be 3992 mm^2, 1656 mm^2 and 127 mm^2 for the 4 l min^{-1}, 2.5 l min^{-1} and 1 l min^{-1} jets respectively. The areas of the RFZ created by the three flow rates on a clean Perspex wall were measured to be 13591 mm^2, 8092 mm^2 and 2893 mm^2 respectively. This shows the extent to which the WSP restricts clean area growth from jet impingement. For a 0.19mm WSP thickness the 1 l min^{-1}, 2.5 l min^{-1} and 4 l min^{-1} clean 4%, 20% and 29% of the area covered by their RFZ on a clean surface respectively. The restriction therefore becomes more discernible at lower flow rates.

Through plotting the ratio A/A*, the removal expressed as a fraction of the maximum removal for a given flow-rate can be examined. This can be expressed in an energy context, through the use of equation 2.3 (with energy being the product of W and time). Fig. 3.5 illustrates that for a given amount of energy, the jet operating at 1 l min^{-1} approaches its long-time area quicker than for the higher flow rates.

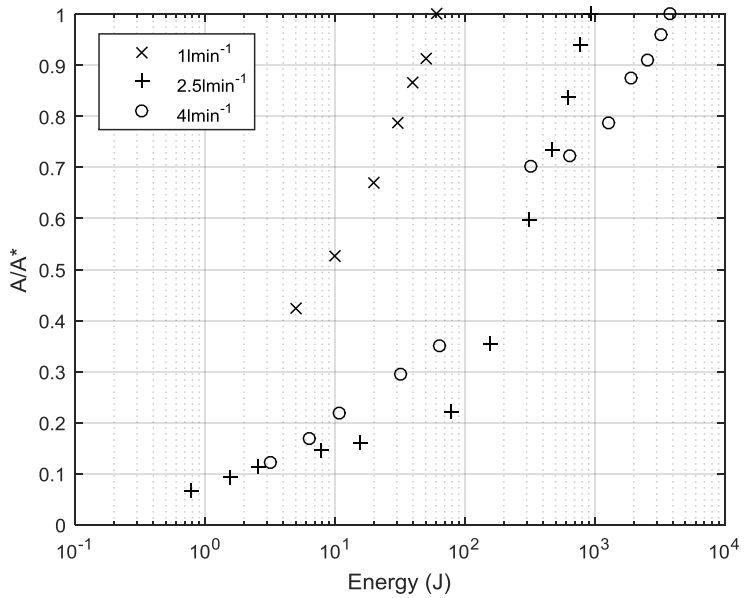

Fig. 3.5: Area relative to final value at each time interval plotted against energy input to the cleaning process (0.19 mm WSP thickness, 20˚C)

A similar approach can be used to give a measure of efficiency defined as cleaned area per unit of energy. This is shown in Fig. 3.6. At short times the removal per unit of energy for the three flow rates is very similar, with efficiencies of material removal being much higher than at longer times. At longer times, jets of a lower flow rate show a greater efficiency in material removal. This is likely due to the difference in the rate of material removal at long times (the gradient of the curves shown in Fig. 3.4), which is lower for the higher flow rates. What can be gleaned from these results is that cleaning should be done in very short bursts as that that is when the efficiency of removal is at its greatest. At short times, cleaning is done in proximity to the impingement point of the jet. In this region shear stresses are at their highest and cleaning is more efficient. As the radial distance from impingement increases the cleaning efficiency reduces since shear stresses on the surface are lower and the ridge of WSP being greater means there is more resistance to clean area growth. For instance the use of a cluster of jets for a short burst of time whose clean areas coalesce would be more efficient than running a single jet for a prolonged time that eventually reaches the same area as the combined area from the cluster.

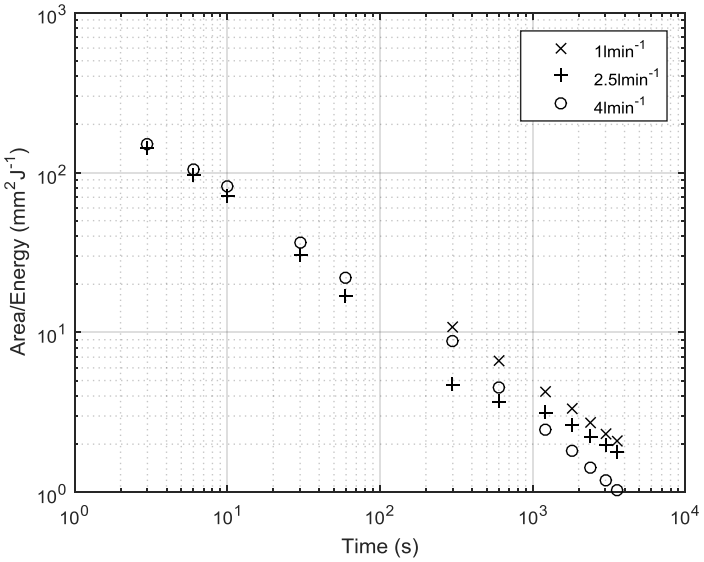

Fig. 3.6: Efficiency of WSP removal from surfaces expressed as clean area per energy (0.19 mm WSP thickness, 20˚C)

3.4 WSP thickness study

To view the effect of WSP thickness on cleaning performance, the WSP thickness was varied between 0.19 mm and 1.9 mm as described in 2.2.2. The resulting clean area versus time graph is shown in Fig. 3.7.

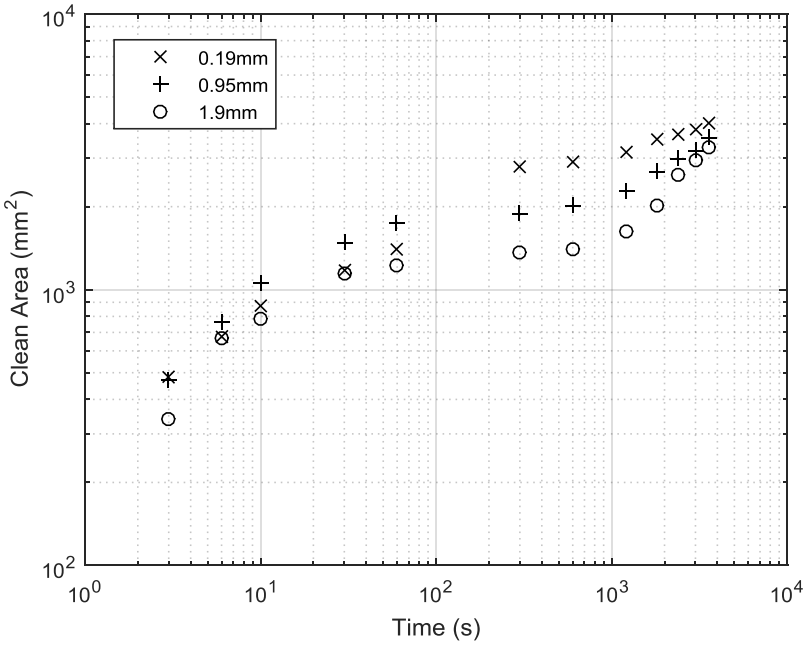

Fig. 3.7: Clean area vs time (4 l min^{-1} flow rate, 20˚C)

For the 4 l min^{-1} flow rate, the cleaning performance during the first minute of operation is very similar for each WSP thickness with all the curves lying close to each other and with a very steep gradient. The curves begin to deviate from one another as the process continues with the lowest WSP thickness showing a higher rate of removal. Ultimately however the final clean areas, A*, reached for each thickness are relatively close together and there is only a 17% discrepancy between the A* value of the 0.19 mm and 1.9 mm WSP thicknesses.

The discrepancy in A* between each thickness becomes more discernible when the flow rate is lowered to 2.5 l min^{-1} (see Fig. 3.8). Once again the clean area curves adhere to a similar gradient in the first minute of cleaning. This is in the region close to the impingement of the jet where shear stresses are such that the thickness of the WSP being cleaned has very little effect on the cleaning performance. However as the radial distance from impingement increases the effect becomes more discernible and the lower flow rates show a notably lower efficiency of removal. There is a 67% reduction in A* when increasing the WSP thickness from 0.19 mm to 1.9 mm.

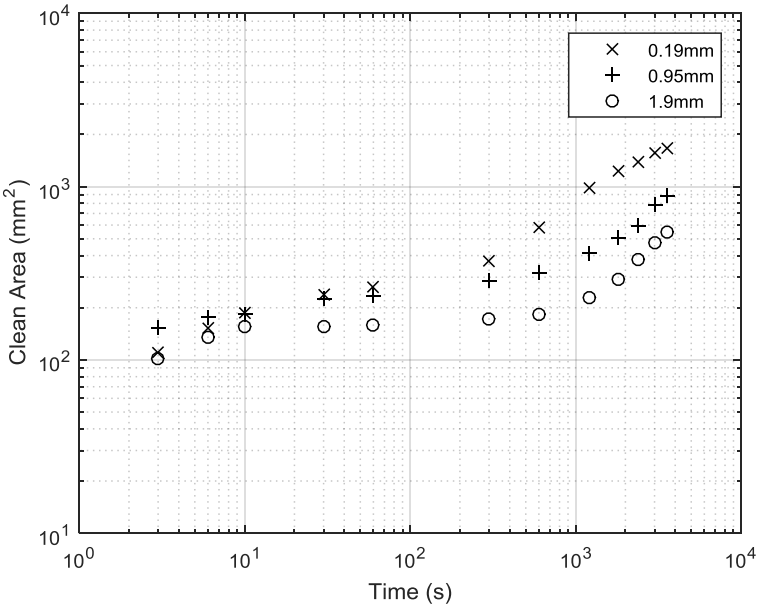

Fig. 3.8: Clean area vs time (2.5 l min^{-1} flow rate, 20˚C)

For the 1 l min^{-1} jet (Fig. 3.9), the breakdown of the soil layer took longer to occur than the higher flow rates due to the force exerted on the layer being lower and taking longer to penetrate to the surface of the wall. As such there are no data points in the first minute of cleaning and the clean area only becomes apparent after 5 minutes. In this case there is a 36% decrease in A* between the 0.19 mm and 1.9 mm WSP thicknesses.

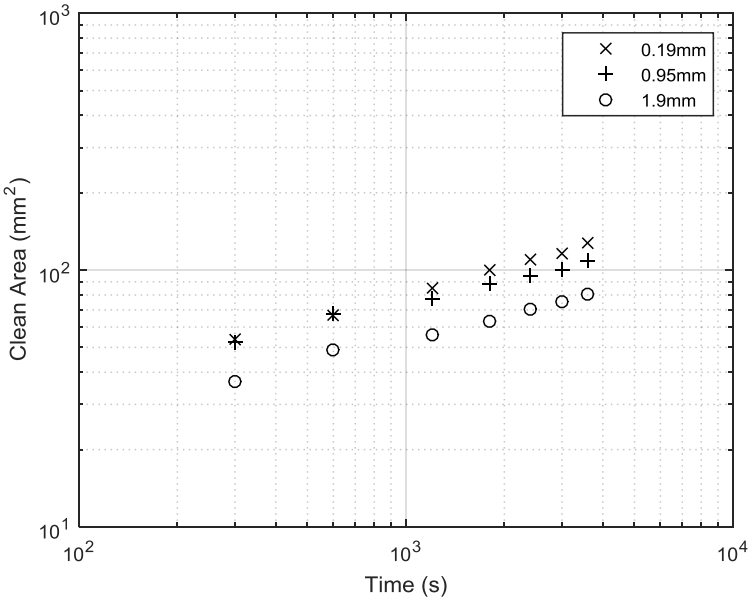

Fig. 3.9: Clean area versus time (1 l min^{-1} flow rate, 20˚C)

3.5 Water temperature study

The temperature of the water was then increased and the experiments repeated at 40 ˚C and 60 ˚C. These experiments were run for 5 minutes as at higher temperatures the majority of cleaning is

achieved in this time and this represents a typical cycle duration on a wash rack. Fig. 3.10 shows the response of clean area vs time for the 4 l min^{-1} jet and 0.95 mm WSP thickness.

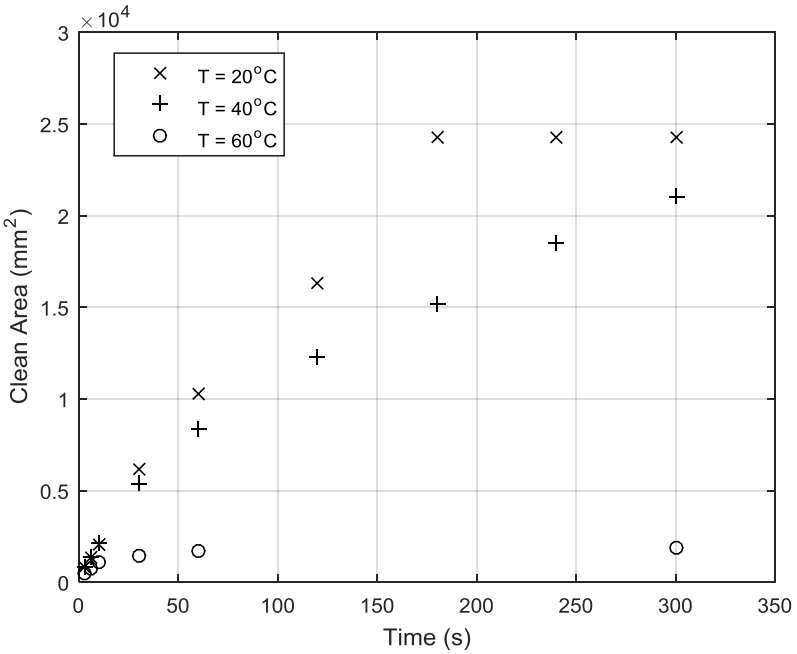

Fig. 3.10: Clean area vs time (4 l min^{-1} flow rate, 0.95 mm WSP thickness)

As the temperature is increased, the cleaning rate increases dramatically, with the clean area reaching a steady value inside 5 minutes of cleaning at 60 ºC. For the first 30 s, the cleaning performance is very similar at 40 and 60 ˚C. Beyond this time, the effect of temperature becomes discernible and the rate of cleaning increases. After 3 minutes, the clean area at 60 ºC has reached its maximum value equating to 24300 mm^2. This is approximately a 500% increase over the value of A* for the 20 ˚C case. 3 minutes of cleaning at 60 ºC sees any WSP on the surface in contact with the hot water is removed as the temperature is above the drop point of the WSP and at this point the material begins to behave more like a liquid than a semi-solid. As such the material is washed away by the falling film created by the jet since the viscosity of the WSP is significantly reduced. At 40 ˚C the time taken to reach its maximum clean area is greater however the final value reached is only slightly smaller than at 60 ˚C, measured to be 21000 mm^2, 13% lower than at 60 ºC. These clean areas both exceed the RFZ created by a 4 l min^{-1} jet on a clean surface, discussed in 3.3, by greater than 50%. This can be explained by the material removed by the falling film. Whilst the melting point of a given WSP is reported across a range of temperatures, reflecting the complexity of the material and multiple phase transitions occurring during heating, targeting the lower end of this range may be appropriate from an energy efficiency perspective since this appears to be sufficient to cause the phase transition to a mobile phase. The loss in structure at this temperature is also observed through rheological measurements by Bentley (2017).

There is also a change in the mechanism of removal of the WSP at these higher temperatures. Fig. 3.11 shows a time lapse series of images of the removal process for the 1 l min^{-1} jet on a 0.95 mm WSP thickness at 60 ˚C. It can be observed there is no formation of a ridge of WSP on the perimeter of the clean area, unlike the case for cleaning below the melting point (Fig. 3.2). After 10 s a very thin layer of material exists between the clean area and the film jump and after 30 s this has been displaced. The growth of the clean area does not significantly increase in width beyond this time, however WSP in the falling film begins to be removed. All material in contact with the jetted fluid is removed from the surface and washed downstream of the flow. The shear stress exerted on the wall by the falling film is great enough to displace the soil.

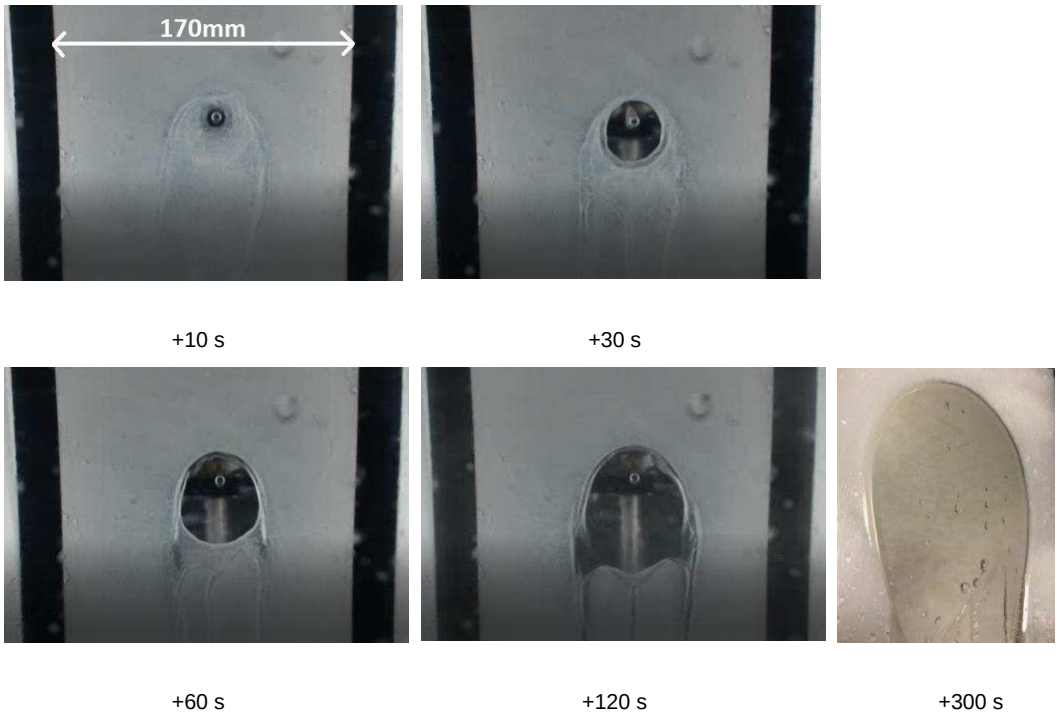

Fig. 3.11: Time lapse of removal 1 l min^{-1} 0.95 mm WSP thickness 60 ^{o}C. (a) 10 s. (b) 30 s. (c) 60 s. (d) 120 s. (e) Zoomed in region of clean area at long time 300 s

4 Conclusions

Both the distribution of flow through a wash-rack and the impact of the jets onto a model surface have been examined. A pipe network approach coupled with visualisation through the use of bubble-plots provides a rapid and easy-to-use method for analysing and optimising the flow through wash racks. As well as demonstrating the application of pipe network theory to this class of problem, this was used to inform typical flow rates through individual nozzles, and the study of single impacting jets onto surfaces. The bubble plot generated from EPANET through modelling of an exemplar rack showed an uneven distribution of flow rates throughout the rack. Certain parts loaded on to these under-supplied nozzles may be the root of cleaning validation failure and the flow distribution can thus be optimised to supply more fluid to these particular nozzles. For the pump curve assumed the flow discharged through the coupling was excessively large but studies showed that this can be significantly reduced by lowering the zero-flow pressure closer to that which is measured downstream of the coupling. To model the flow through the coupling with a degree of certainty, it is essential that the pump characteristics applied are known to be accurate. Once this is the case the method used is a useful framework for rack optimisation, as it is entirely plausible that discharge through the coupling still exceeds that which is necessary for self-cleaning purposes.

For the removal of white-soft paraffin, with temperatures below the drop-point of the material, the mechanism of displacement of soil from the surface was suggested to be through a roll-up process and the majority of soil remains in the ridge around the impingement zone. At higher temperatures and above the drop point of the WSP the mechanism at which soil was removed was different. Here the rheology of the WSP changed such that the majority of material in contact with the flow was washed away and the thickness of the surrounding WSP was unaltered. A definition of cleaning within an energy efficiency framework, that being the energy for the flow to be driven through the nozzle and neglecting thermal energy, is established and this suggests that the most efficient removal of soil is at the start of the process, where the shear stress on the surface is greatest. Using an energy approach and integrating this with flow through a rack will allow subsequent optimisation of jet number, placement,

flow rate and water temperature for more efficient cleaning of surfaces on wash racks used in the manufacture of pharmaceuticals. For instance; in the standoff distance range studied (<200 mm), the results presented show how the use of short bursts of a jet are far more efficient from an energy perspective. As the results of Fig. 3.6 showed, the efficiency of the process decreases considerably with time as the radial distance from impingement increases and lower shear stresses exerted on the surface further away from impingement leads to inefficient cleaning. Relating this to the wash rack, cleaning using a cluster of short burst jets whose clean areas coalesce would provide more efficient cleaning than a single jet which eventually reaches the same area as the cluster, given enough time. Cycle times could be reduced and energy usage would be considerably lowered. Also the results have shown that for WSP based products, it is possible that water temperatures on the rack could be reduced. As long as the drop point of the WSP is exceeded, the temperature is sufficient enough to cause phase transition to a mobile phase and as such the vast majority of material in contact with the flow is removed from the surface.

Acknowledgements

GlaxoSmithKline and The University of Leeds are gratefully acknowledged for supporting the studentship of Alistair Rodgers. GlaxoSmithKline and Royal Academy of Engineers are thanked for supporting the Research Chair of Nik Kapur. Thank you also to Emma Krop of The University of Leeds for assisting with the penetrometer testing of the WSP.

Nomenclature

A	Clean area (mm^2)
A*	Long-time clean area (1 hour) (mm^2)
CIP	Cleaning-in-place
COP	Cleaning-out-of-place
d	Nozzle standoff distance (mm)
k	Nozzle discharge coefficient ($l\ min^{-1}Pa^{-0.5}$)
MACO	Maximum allowable carry over
ΔP	Pressure drop across the nozzle (Pa)
Q	Flow rate ($l\ min^{-1}$)
RFZ	Radial flow zone
t	Tape thickness (mm)
T	Water temperature (^oC)
W	Power (W)
WSP	White soft paraffin

References

Bentley, P.J. (2017) Investigation of the Functionality of White Soft Paraffin with Regards to Ointments. PhD thesis, University of Leeds, pp.80-90

Box, G., Behnken, D. (1960) Some New Three Level Designs for the Study of Quantitative Citation Variables, Technometrics, 2, pp.455-475

Drosos, E.I.P, Paras, S.V., Karabelas, A.J. (2004) Characteristics of Developing Free Falling Films at Intermediate Reynolds and High Kapitza Numbers, International Journal of Multiphase Flow, 30, pp.853-876

Engineering ToolBox (2004) Power Gained by Fluid from Pump or Fan. Available online: https://www.engineeringtoolbox.com/pump-fan-power-d_632.html [18th August 2018].

Food and Drug Administration (FDA) (1993) Guide to Inspections Validation of Cleaning Processes

Fryer, P.J., Asteriadou, K. (2009) A prototype cleaning map: A classification of industrial cleaning processes, Trends in Food Science & Technology 20, pp.255-262

Lakshmana Prabu, S., Suriyaprakash, T.N.K. (2010) Cleaning Validation and its Importance in Pharmaceutical Industry. Pharma Times, 42(7), pp.21-24

McLaughlin, M.C., Zisman, A.S. (2005) The Aqueous Cleaning Handbook: A Guide to Critical-Cleaning Procedures, Techniques, and Validation, p.25

Pharmacopoeia, E. (2005) 2.9.9. Measurement of Consistency by Penetrometry In: European Pharmacopoeia 5.0., pp.235-237

Pharmaceutical Manufacturing Technology Centre (PMTC). (2015) Good Cleaning Validation Practice, pp.6-15

Rasband, W.S. (1997) ImageJ, U.S. National Institutes of Health, Bethesda, Maryland, USA, Available online: https://imagej.nih.gov.ij/

Rosen, M.J., Kunjappu, J.T. (2012) Surfactants and Interfacial Phenomena, 3rd edition, pp.1-6

Rossman (2000) EPANET 2 Users Manual, p.29

Shewale, D.S., Chavan, M., Parek, S.S. (2014) Pharmaceutical Product Recall: Lesson Learned, International Pharmaceutical Industry, 6 (1), pp.16-17

Shimbun, N.K. (1988) Poka-Yoke: Improving Product Quality by Preventing Defects, Productivity Press, p.111

Sinner, H. (1959) The Sinner Circle “TACT.” Sinner’s Cleaning Philosophy. Henkel

Tailby, S. R., Portalski, S. (1961) The optimum concentration of surface active agents for the suppression of ripples, Transactions of the Institution of Chemical Engineers, 39, pp.328-336

Todini, E., Pilati, S. (1988) A gradient method for the analysis of pipe networks. International Conference on Computer Applications for Water Supply and Distribution, Leicester Polytechnic, UK, September 8-10.

United States Environmental Protection Agency, USA (2016). EPANET [Computer software]. Available online: https://www.epa.gov/water-research/epanet.

Wilson, D.I., Le, B.L., Dao, H.D.A., Lai, K.Y., Morison, K.R., Davison, J.F. (2012) Surface flow and drainage films created by horizontal impinging liquid jets, Chemical Engineering Science, 68, pp.449-460

Wilson, D.I., Atkinson, P., Kohler, H., Mauermann, M., Stoye, H., Suddaby, K., Wang, T., Davidson, J.F., Majschak, J.P. (2014) Cleaning of Soft-Solid Soil Layers on Vertical and Horizontal Surfaces by Stationary Coherent Impinging Liquid Jets, Chemical Engineering Science, 109, pp.184-186